Proton Segregation and Space-Charge at the $BaZrO_3$ (0 0 1)/MgO (0 0 1) heterointerface

Jonathan M. Polfus[a*], Truls Norby[b], Rune Bredesen[a]

[a]SINTEF Materials and Chemistry, PO Box 124 Blindern, NO-0314 Oslo, Norway
[b]Department of Chemistry, University of Oslo, Centre for Materials Science and Nanotechnology (SMN), FERMiO, Gaustadalléen 21, NO-0349 Oslo, Norway

*Contact email: jonathan.polfus@sintef.no

Abstract

Y-doped $BaZrO_3$ (BZY) can be deposited epitaxially on MgO (0 0 1) and the considered interface serves as a model system for studying heterointerface properties of protonic conductors. In this study, the defect chemistry of the interface between $BaZrO_3$ (0 0 1) and MgO (0 0 1) was investigated by first-principles calculations and space-charge theory. Segregation energies from the BZY bulk to the interface ZrO_2 and MgO layers were calculated for effectively charged protons, oxygen vacancies, Y-acceptors as well as cation vacancies. Protons were found to exhibit a strong tendency for segregating to the interface, particularly to an oxide ion in the MgO layer, rendering a net positive charge of the interface. According to the applied thermodynamic space-charge models, the interface potential could reach more than 1 V under the Mott-Schottky approximation, with depletion regions extending up to 2 nm into BZY. With fully equilibrated Y-segregation profiles, the interface potential was significantly diminished to about 0.2 V at 573 K and 0.025 bar H_2O. While the interface was found to be close to saturated by protons under most condition, it was concluded that proton conduction along the interface could not contribute significantly to the in-plane conductivity of BZY films deposited on MgO substrate.

Keywords: barium zirconate; thin film; substrate interface; space-charge; density functional theory;

1. Introduction

Acceptor doped barium zirconate is a promising proton-conducting ceramic electrolyte for application in fuel cells and electrolyzers due to its high protonic conductivity at intermediate temperatures (400-600 °C) and chemical stability towards CO_2 [1–4]. $BaZrO_3$-based electrolytes have recently also been integrated as electrochemical membranes in catalytic co-ionic membrane reactors for dehydroaromatization [5]. Grain boundaries, surfaces and heterointerfaces are regions of particular interest in such electrochemical devices. Considering the overall ionic transport properties of these materials, metal cation transport may in particular be *facilitated along* interfaces, while transport of protons and oxide ions may be *impeded across* interfaces [6]. For instance, the grain boundary resistance in Y-doped $BaZrO_3$ (BZY) has been ascribed to the depletion of protons in space-charge regions adjacent to a positively charged interface [7–15]. According to the space-charge model, the depletion region originates from segregation of oxygen vacancies and protons to the structurally distorted grain boundary, yielding an interface of net positive charge. Space-charge models have recently also been applied to describe the defect chemistry of $BaZrO_3$

surfaces which were found to exhibit subsurface depletion regions [16,17] and adsorbed hydroxide ions have recently been shown to play an important role [18].

A heterointerface can be considered as a similarly distorted structure with imperfect coordination polyhedra, and can therefore be expected to exhibit space-charge regions. In an electrolyte-electrode heterointerface, both phases exhibit large concentrations of ionic and/or electronic charge carriers. The charged core of the phase boundary can then be charge compensated by (asymmetric) space-charge layers extending into both phases. For a heterointerface between a doped material and an undoped substrate, the interface potential will mainly be determined by the phase with the largest concentration of effectively charged point defects, e.g., a doped electrolyte or electrode material. This is because the doped material has a larger capacity to compensate the interface charge in the form of space-charge regions for a given interface potential.

Heterointerfaces have been suggested to give rise to particularly high proton conductivities in thin BZY films on MgO (0 0 1) and $NdGaO_3$ (1 1 0) substrates due to misfit dislocations and texturing in the BZY material [19,20]. Thin films of BZY can be deposited epitaxially on MgO (0 0 1) substrates due to the excellent lattice match within about 0.25% and both BaO and ZrO_2 terminations have been observed [19,21]. The ZrO_2 termination comprises complete ZrO_6 and MgO_6 octahedra across the interface. The difference in structure between perovskite $BaZrO_3$ (space group $Pm\bar{3}m$) and rock-salt MgO ($Fm\bar{3}m$) results in an exposed oxide ion in the MgO layer which is not coordinated to any cations in $BaZrO_3$ (see Figure 1). This special interface oxide ion in the MgO layer can therefore be considered to resemble a MgO (0 0 1) surface oxide ion. On the other hand, the atomistic structure of the BaO-terminated interface is less coherent and can be expected to comprise a larger degree of non-stoichiometry and/or coordination polyhedra that differ from the bulk structure of the respective materials.

Electrical characterization of thin films is inherently difficult due the possible contributions to in-plane conductivities from the interface and substrate material. The film-substrate interface may give rise to new ionic and electronic conduction paths, and space-charge effects can significantly alter the charge carrier concentrations close to the interface. In the present work, space-charge effects were evaluated for the ZrO_2-terminated BZY (0 0 1)/MgO (0 0 1) heterointerface by first principles calculations. The BaO-terminated interface was not considered due the uncertainty regarding its atomistic structure and stoichiometry. Point defects were introduced to the pristine interface and the role of dislocation or other texturing was not investigated. MgO was selected as the inert substrate due to its low concentration of bulk point defects compared to the 10 mol% acceptor doped $BaZrO_3$. The potential and concentration profiles of point defects were considered across the interface as function of temperature for given atmospheric conditions with particular emphasis on protons, oxygen vacancies and Y-acceptors, i.e., $\mathrm{OH}_{\mathrm{O}}^{\bullet}$, $\mathrm{v}_{\mathrm{O}}^{\bullet\bullet}$, and $\mathrm{Y}_{\mathrm{Zr}}^{/}$ in Kröger-Vink notation [22]. The structural interface, or core, was defined in the atomistic models as the ZrO_2 and MgO layer and termed *interface*, while the space-charge region refers to the depletion/accumulation region of non-zero potential adjacent to the structural interface. Both the interface and space-charge region can exhibit charge carrier concentrations and mobilities different from bulk, and thus, they can both contribute to the properties of the electrical interface characterized experimentally.

2. Computational approach

The interface was constructed with a thickness of 5 unit cells (11 layers) for each material, and the cell contained two equivalent interfaces due to the periodic boundary conditions. The lattice parameter was fixed to that of MgO to represent a thin $BaZrO_3$ film adapting to a rigid MgO substrate. The distance between the two materials was optimized in steps of 0.1 Å.

Calculations with point defects were performed in supercells with 3 x 3 expansion in the ab-plane and a total of 648 atoms. Defect segregation energies, $\Delta E_i^{\mathrm{seg}}$, were calculated as the total energy difference for the defect between the interface and the bulk $BaZrO_3$ region in the same cell, i.e., at least 5 atomic layers or 10.5 Å away from the interface. Spurious interactions between the point defect and its period image, as well as the electrostatic interaction with the uniform background charge present in cells containing charged defects, can therefore be assumed to be canceled out for $\Delta E_i^{\mathrm{seg}}$. The bulk defect equilibria in $BaZrO_3$ were determined from the simplified electroneutrality, $c_{\mathrm{Y}'_{\mathrm{Zr}}} = 2c_{\mathrm{v}_{\mathrm{O}}^{\bullet\bullet}} + c_{\mathrm{OH}_{\mathrm{O}}^{\bullet}}$, and a constant 10 mol% Y-acceptor concentration. The enthalpy and entropy of hydration was taken as -0.72 eV and -1.00 meV K^{-1}, respectively [23].

The defect segregation energies were implemented in a space-charge model based on a constant electrochemical potential of all species across bulk, interface, space-charge region and gas phase [9,24–29]. The same approach has been applied to coherent grain boundaries and surfaces of $BaZrO_3$ [14,30–32]. The dilute limit treatment of the point defects can be considered the most significant approximation within this computational approach and thermodynamic implementation. Interaction between defects was considered for protons at the interface (Section 3.3), and can in general be expected to limit defect accumulation at the interface. A dielectric constant of 75 was chosen based on reported values for Y-doped $BaZrO_3$ ceramics [3,7,8,33,34].

DFT calculations were performed using the projector-augmented wave (PAW) method [35] as implemented in VASP [36] with the generalized gradient approximation (GGA) functional due to Perdew, Burke and Ernzerhof [37]. Geometric optimization of the unit cells was performed with a 500 eV plane-wave energy cut-off, and subsequent defect calculations were performed in supercells with fixed lattice parameters and a 400 eV plane-wave energy cut-off. k-point sampling was done according 2 x 2 x 1 Monkhorst-Pack scheme for the supercell [38]. The ionic positions were optimized until the residual forces were within 0.02 eV $Å^{-1}$, while the self-consistent electronic optimization was performed with an energy convergence criterion of 10^{-6} eV.

3. Results and discussion

3.1 Interface structure

Figure 1 shows the relaxed structure of the interface which exhibits only minor distortions. The optimized Mg/Zr–O bond lengths were slightly elongated at the interface, 2.21-2.24 Å compared to approx. 2.14 Å in the bulk regions of both $BaZrO_3$ and MgO. According to the relaxed lattice parameter of MgO, 4.226 Å, $BaZrO_3$ was subjected to a compressive strain of less than 0.002. The interface structure contains one site for each of the cations. There are three different oxide ion sites: 1) in the ZrO_2 layer; 2) in the MgO layer coordinated to Zr^{4+}; and 3) in the MgO layer without coordination to $BaZrO_3$ (Figure 1).

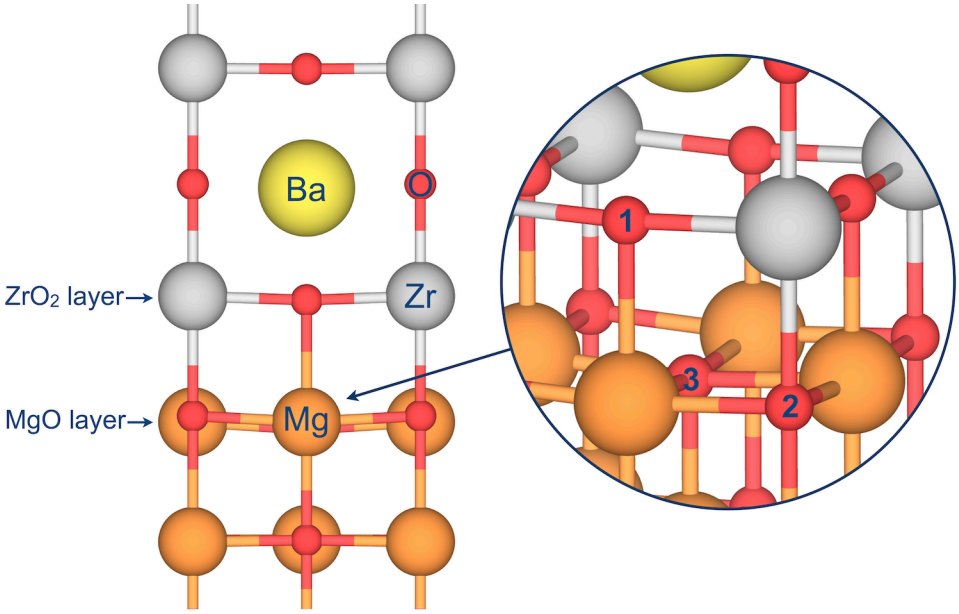

Figure 1: Relaxed structure of the interface with a highlight showing the three different oxide ion sites.

3.2 Defect segregation energies

Figure 2 shows the relaxed local structure and corresponding segregation energies of $OH_O^{\bullet}$ and $v_O^{\bullet\bullet}$ relative to the bulk region of $BaZrO_3$. Protons exhibited a large stabilization in the interface ZrO_2 layer (Figure 2a, left) with a segregation energy of -0.90 eV. The proton relaxed away from the equilibrium position in bulk (within the ZrO_2-plane) towards a position otherwise occupied by Ba^{2+}. The large stabilization may therefore be associated with the steric repulsion between $OH_O^{\bullet}$ and the A-site cation in perovskites [39] as evident from the rather large binding energy between barium vacancies and protons [40]. The stabilization of $OH_O^{\bullet}$ was even larger in the interface MgO layer (Figure 2a, right) with a segregation energy of -1.40 eV. A similar proton position was reported for dissociatively adsorbed water on the MgO (0 0 1) surface [41]. In comparison, the segregation energy of $OH_O^{\bullet}$ from the bulk region of $BaZrO_3$ to the bulk region of MgO was +0.58 eV. Oxygen vacancies exhibit a slight stabilization in the interface ZrO_2 layer and a sizeable stabilization in the interface MgO layer with a segregation energy of -0.52 eV (Figure 2b). The segregation energy of $v_O^{\bullet\bullet}$ to the Zr-coordinated oxide ion site in the MgO layer was +1.54 eV, i.e., even more positive than segregation to the bulk MgO region, 1.04 eV.

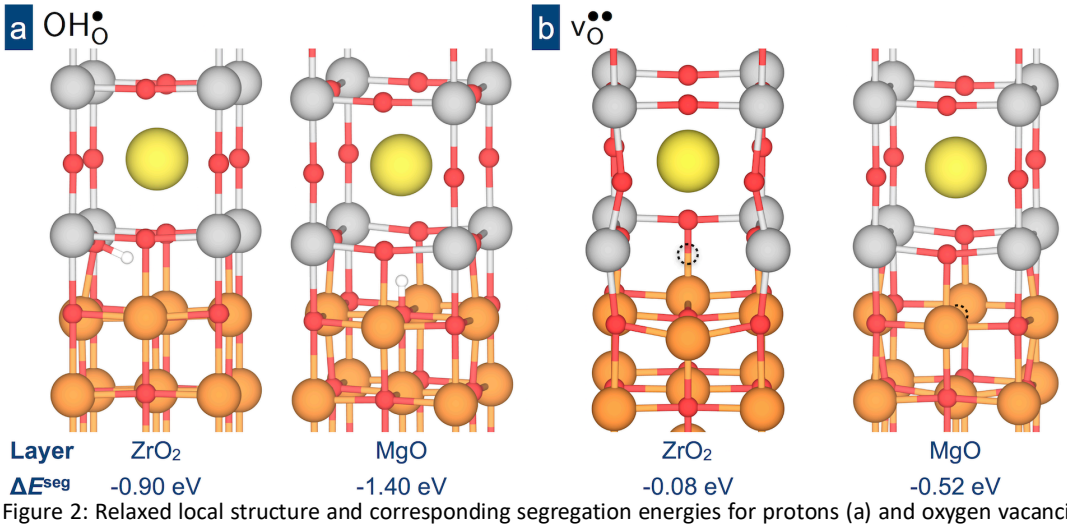

Figure 2: Relaxed local structure and corresponding segregation energies for protons (a) and oxygen vacancies (b) relative to bulk $BaZrO_3$.

Figure 3 shows the relaxed local structure and corresponding segregation energies of cation defects at the interface. The segregation energy of Y'_{Zr} was close to zero, that of barium vacancies was slightly positive. Zirconium vacancies exhibited a slightly negative segregation energy of -0.20 eV. On the other hand, magnesium vacancies were significantly stabilized at the interface with a segregation energy of -0.77 eV. Intermixing between the ZrO_2 and MgO layer at the interface was evaluated according to the reaction

$$Zr_{Zr}^{\times} + Mg_{Mg}^{\times} = Zr_{Mg}'' + Mg_{Zr}^{\bullet\bullet} \quad (1)$$

with a calculated enthalpy of 0.39 eV. Accordingly, the degree of intermixing can be expected to be rather insignificant particularly for thin films deposited at intermediate temperatures.

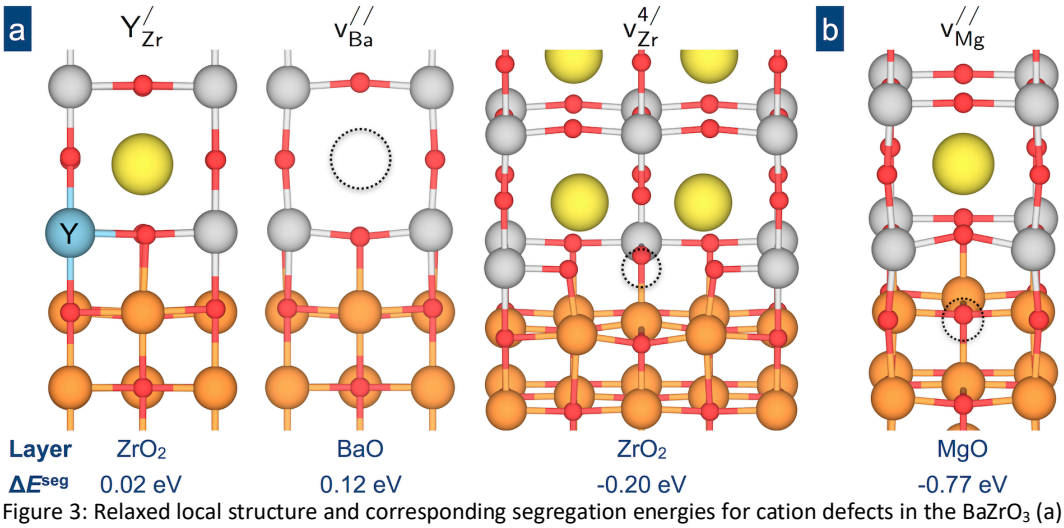

Figure 3: Relaxed local structure and corresponding segregation energies for cation defects in the $BaZrO_3$ (a) and MgO part (b) of the interface.

3.3 Space-charge properties

The influence of a specific defect on the space-charge characteristics of the interface can be defined by two main factors. Firstly, the tendency for the defect to accumulate at the interface is largely determined by the defect segregation energy. Together with the

effective charge of the defect in relation to the interface potential, as well as the bulk defect concentration, the segregation energy determines the defect's contribution to the overall charge of the structural interface. Secondly, the bulk concentration and charge of the defect determines to which extent the defect can influence the overall charge of the space-charge region by accumulating or depleting. Thus, while defects of low bulk concentration may accumulate at the interface, it is only the defects that predominate in bulk that contribute significantly to the total charge of the space-charge region.

The most important defects in the current system are therefore $OH_O^{\bullet}$ and $v_O^{\bullet\bullet}$ due to their large negative segregation energies and bulk concentrations, yielding a positive core potential. Consequently, $Y_{Zr}^{/}$ becomes increasingly important at the interface due to its electrostatic stabilization despite the insignificant segregation energy of 0.02 eV. Furthermore, $Y_{Zr}^{/}$ exhibits the largest bulk concentration and is therefore the largest contributor to the charge of the space-charge region by accumulating according to the potential profile. Another important consideration is whether the cation defects are allowed to fully equilibrate at the interface and in the space-charge region. The Mott-Schottky approximation – assuming a constant acceptor concentration throughout – is often applied to represent a frozen concentration of $Y_{Zr}^{/}$ from fabrication of the material, while more mobile defects such as $OH_O^{\bullet}$ and $v_O^{\bullet\bullet}$ are allowed to equilibrate. The treatment of $Y_{Zr}^{/}$ was found to be crucial for the space-charge properties of the system in accordance with previous studies [18,29], and the most reasonable description is expected to lie in between these two extreme cases depending on the thermal history of the material. Thus, while $v_{Mg}^{//}$ exhibits a strong tendency for accumulating at the interface, the low bulk concentration means that it does not have any influence in the space-charge region, and $v_{Mg}^{//}$ was therefore not considered for simplicity. The cation vacancies in $BaZrO_3$ exhibit low bulk concentrations and positive segregation energies, and were therefore also not considered further. The concentration of protons at the interface was limited to 1 per formula unit $BaZrO_3$ or MgO due to the close proximity between the $OH_O^{\bullet}$ site in the MgO and ZrO_2 layer (Figure 2a) so that both sites cannot be occupied simultaneously.

Figure 4 shows defect concentrations and potential at the interface as function of distance in the space-charge region at 573 K and 973 K, corresponding to hydrated and dehydrated bulk, respectively, with a constant concentration of $Y_{Zr}^{/}$. The interface is close to saturated with $OH_O^{\bullet}$ irrespective of the predominating defect in bulk due to the remarkably negative segregation energy for protons. The space-charge potentials become quite large, 1.17 V and 0.90 V, respectively, in order to achieve sufficient depletion of the effectively positive defects in the space-charge region to compensate the surface charge. The temperature dependence of the space-charge potential was close to linear, from 1.2 V at 373 K to 0.6 V at 1273 K for the Mott-Schottky approximation. The lower space-charge potential at higher temperature mainly originates from the reduced bulk proton concentration due to dehydration, and consequently, lower interface proton concentration and positive charge (Figure 4).

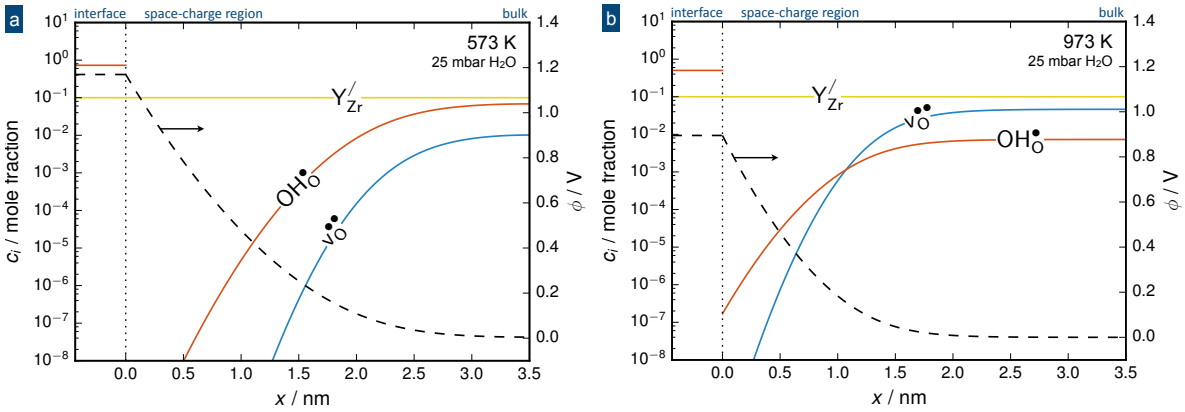

Figure 4: Defect concentrations at the interface and as function of distance into the space-charge region in BZY at 573 K (a) and 973 K (b) within the Mott-Schottky approximation.

The concentration profile of Y'_{Zr} is fully equilibrated at 573 K in Figure 5, for comparison with Figure 4a. While the interface is now fully saturated with protons, accumulation of Y'_{Zr} at the interface and in the space-charge region results in a substantially diminished surface potential of 0.16 V. Accordingly, the overall depletion of $OH^{\bullet}_{O}$ and $v^{\bullet\bullet}_{O}$ in the space-charge region becomes significantly lower. The space-charge potential increased to 0.24 V at 1273 K with fully equilibrated Y'_{Zr}. The concentration of Y'_{Zr} at the interface and in the space-charge region can, however, be expected to be limited by the Y-dopant solubility in $BaZrO_3$ and the strain induced at the interface at high concentrations, in addition to the kinetic limitations due to slow cation diffusion. Experimental evidence has shown clear dopant accumulation close to positively charged grain boundaries in Y-doped and Sc-doped $BaZrO_3$ [11,42–44]. The dopant accumulation was less pronounced than the profile in Figure 5, and electrical characterization implied a decreased space-charge potential.

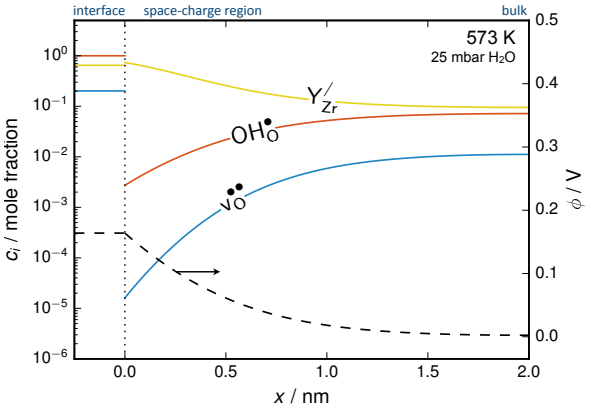

Figure 5: Defect concentration at the interface and as function of distance into the space-charge region of BZY with Y-acceptor fully equilibrated to the potential profile.

The proton conduction properties of BZY at the interface can be evaluated by considering the depletion of protons in the space-charge region, and the accumulation of protons at the interface layer. For a BZY film deposited on a MgO substrate, the effective thickness of the film would be reduced by approx. 1-2 nm according to the thickness of the depletion region for an in-plane measurement. Conduction along the interface can also be considered since the interface MgO layer (Figure 2a) is close to saturated with protons under most conditions. The proton sites in the MgO layer are not directly connected and proton migration must therefore involve the adjacent ZrO_2 layer. Relative to the -1.40 eV

position in the MgO layer, the thermodynamic stability of protons was 0.5 eV higher in the interface ZrO_2 layer (Figure 2a, left) and 1.0 eV higher associated with the same oxide ion but directed into $BaZrO_3$, which is necessary for rotation and diffusion to the adjacent MgO layer site. Thus, the activation energy for proton conductivity along the interface layer is according to these calculations at least 1 eV. Despite the high proton concentration, the interface MgO layer can therefore not be expected to contribute to the in-plane proton conductivity of BZY films on MgO due to the reduced symmetry of the interface proton sites. On the other hand, one may speculate whether the significant space-charge potential of the investigated interface can give rise to significant in-plane n-type conductivity due to accumulation of electrons along the interface under reducing conditions.

4. Conclusions

The $BaZrO_3$/MgO (0 0 1) interface was found to exhibit a strong tendency for proton accumulation, in part due to a special proton position associated with the oxide ion in the interface MgO layer. The strong tendency of this oxide ion for being protonated may be ascribed to its resemblance to the MgO (0 0 1) surface oxide ion, as it has no bonds to $BaZrO_3$, and therefore is not fully coordinated. The interface attained a net positive charge, and the interface potential could exceed 1 V according to the applied thermodynamic models under the Mott-Schottky approximation. The space-charge region and depletion of protons extended up to 2 nm from the interface. The treatment of Y-acceptor dopant was found to be crucial for the space-charge characteristics: the interface potential diminished to approx. 0.2 eV when Y was allowed to fully equilibrate by accumulating at the interface and in the space-charge region.

5. Acknowledgements

Financial support from the Research Council of Norway, project Nano2021/228355 "Functional oxides for clean energy technologies: fuel cells, gas separation membranes and electrolysers" (FOXCET) conducted by SINTEF Materials and Chemistry, University of Oslo, and NTNU, is gratefully acknowledged. Computational resources were provided by the Norwegian Metacenter for Computational Science (NOTUR) under the projects nn9259k.

6. References

[1] H. Iwahara, T. Yajima, T. Hibino, K. Ozaki, H. Suzuki, Protonic conduction in calcium, strontium and barium zirconates, Solid State Ionics. 61 (1993) 65–69. doi:10.1016/0167-2738(93)90335-Z.

[2] K.D. Kreuer, S. Adams, W. Münch, A. Fuchs, U. Klock, J. Maier, Proton conducting alkaline earth zirconates and titanates for high drain electrochemical applications, Solid State Ionics. 145 (2001) 295–306. doi:10.1016/S0167-2738(01)00953-5.

[3] Y. Yamazaki, R. Hernandez-Sanchez, S.M. Haile, High total proton conductivity in large-grained yttrium-doped barium zirconate, Chem. Mater. 21 (2009) 2755–2762. doi:10.1021/cm900208w.

[4] C. Duan, J. Tong, M. Shang, S. Nikodemski, M. Sanders, S. Ricote, A. Almansoori, R. O'Hayre, Readily processed protonic ceramic fuel cells with high performance at low temperatures, Science. 349 (2015) 1321–1326. doi:10.1126/science.aab3987.

[5] S.H. Morejudo, R. Zanon, S. Escolastico, I. Yuste-Tirados, H. Malerød-Fjeld, P.K. Vestre, W.G. Coors, A. Martinez, T. Norby, J.M. Serra, C. Kjølseth, Direct conversion of

methane to aromatics in a catalytic co-ionic membrane reactor, Science. 353 (2016) 563–566. doi:10.1126/science.aag0274.

[6] J. Maier, Defect chemistry and ion transport in nanostructured materials: Part II. Aspects of nanoionics, Solid State Ionics. 157 (2003) 327–334. doi:10.1016/S0167-2738(02)00229-1.

[7] C. Kjølseth, H. Fjeld, Ø. Prytz, P.I. Dahl, C. Estournès, R. Haugsrud, T. Norby, Space–charge theory applied to the grain boundary impedance of proton conducting $BaZr_{0.9}Y_{0.1}O_{3-\delta}$, Solid State Ionics. 181 (2010) 268–275. doi:10.1016/j.ssi.2010.01.014.

[8] C.-T. Chen, C.E. Danel, S. Kim, On the origin of the blocking effect of grain-boundaries on proton transport in yttrium-doped barium zirconates, J. Mater. Chem. 21 (2011) 5435. doi:10.1039/c0jm03353g.

[9] R.A. De Souza, Z.A. Munir, S. Kim, M. Martin, Defect chemistry of grain boundaries in proton-conducting solid oxides, Solid State Ionics. 196 (2011) 1–8. doi:10.1016/j.ssi.2011.07.001.

[10] F. Iguchi, C.-T. Chen, H. Yugami, S. Kim, Direct evidence of potential barriers at grain boundaries in Y-doped $BaZrO_3$ from dc-bias dependence measurements, J. Mater. Chem. 21 (2011) 16517. doi:10.1039/c1jm12685g.

[11] M. Shirpour, R. Merkle, C.T. Lin, J. Maier, Nonlinear electrical grain boundary properties in proton conducting Y-$BaZrO_3$ supporting the space charge depletion model., Phys. Chem. Chem. Phys. 14 (2012) 730–40. doi:10.1039/c1cp22487e.

[12] M. Shirpour, R. Merkle, J. Maier, Space charge depletion in grain boundaries of $BaZrO_3$ proton conductors, Solid State Ionics. 225 (2012) 304–307. doi:10.1016/j.ssi.2012.03.026.

[13] M. Shirpour, R. Merkle, J. Maier, Evidence for space charge effects in Y-doped $BaZrO_3$ from reduction experiments, Solid State Ionics. 216 (2012) 1–5. doi:10.1016/j.ssi.2011.09.006.

[14] J.M. Polfus, K. Toyoura, F. Oba, I. Tanaka, R. Haugsrud, Defect chemistry of a $BaZrO_3$ Σ3 (111) grain boundary by first principles calculations and space-charge theory., Phys. Chem. Chem. Phys. 14 (2012) 12339–46. doi:10.1039/c2cp41101f.

[15] B. Joakim Nyman, E.E. Helgee, G. Wahnström, Oxygen vacancy segregation and space-charge effects in grain boundaries of dry and hydrated $BaZrO_3$, Appl. Phys. Lett. 100 (2012) 61903. doi:10.1063/1.3681169.

[16] J.-S. Kim, J.-H. Yang, B.-K. Kim, Y.-C. Kim, Proton conduction at BaO-terminated (001) $BaZrO_3$ surface using density functional theory, Solid State Ionics. 275 (2015) 19–22. doi:10.1016/j.ssi.2015.03.021.

[17] T.S. Bjørheim, M. Arrigoni, S.W. Saeed, E. Kotomin, J. Maier, Surface segregation entropy of protons and oxygen vacancies in $BaZrO_3$, Chem. Mater. 28 (2016) 1363–1368. doi:10.1021/acs.chemmater.5b04327.

[18] J.M. Polfus, T.S. Bjørheim, T. Norby, R. Bredesen, Surface defect chemistry of Y-substituted and hydrated $BaZrO_3$ with subsurface space-charge regions, J. Mater. Chem. A. 4 (2016) 7437–7444. doi:10.1039/C6TA02067D.

[19] D. Pergolesi, E. Fabbri, A. D'Epifanio, E. Di Bartolomeo, A. Tebano, S. Sanna, S. Licoccia, G. Balestrino, E. Traversa, High proton conduction in grain-boundary-free yttrium-doped barium zirconate films grown by pulsed laser deposition, Nat. Mater. 9 (2010) 846–852. doi:10.1038/nmat2837.

[20] N. Yang, C. Cantoni, V. Foglietti, A. Tebano, A. Belianinov, E. Strelcov, S. Jesse, D. Di Castro, E. Di Bartolomeo, S. Licoccia, S. V. Kalinin, G. Balestrino, C. Aruta, Defective

Interfaces in Yttrium-Doped Barium Zirconate Films and Consequences on Proton Conduction, Nano Lett. 15 (2015) 2343–2349. doi:10.1021/acs.nanolett.5b00698.
[21] S.B. Mi, C.L. Jia, M.I. Faley, U. Poppe, K. Urban, High-resolution electron microscopy of microstructure of $SrTiO_3$/$BaZrO_3$ bilayer thin films on MgO substrates, J. Cryst. Growth. 300 (2007) 478–482. doi:10.1016/j.jcrysgro.2006.12.026.
[22] F.A. Kröger, H.J. Vink, Relations between the Concentrations of Imperfections in Crystalline Solids, Solid State Phys. - Adv. Res. Appl. 3 (1956) 307–435.
[23] T.S. Bjørheim, E.A. Kotomin, J. Maier, Hydration entropy of $BaZrO_3$ from first principles phonon calculations, J. Mater. Chem. A. 3 (2015) 7639–7648. doi:10.1039/C4TA06880G.
[24] K. Lehovec, Space-Charge Layer and Distribution of Lattice Defects at the Surface of Ionic Crystals, J. Chem. Phys. 21 (1953) 1123. doi:10.1063/1.1699148.
[25] K.L. Kliewer, J.S. Koehler, Space Charge in Ionic Crystals. I. General Approach with Application to NaCl, Phys. Rev. 140 (1965) A1226. doi:10.1103/PhysRev.140.A1226.
[26] J. Jamnik, J. Maier, S. Pejovnik, Interfaces in solid ionic conductors: Equilibrium and small signal picture, Solid State Ionics. 75 (1995) 51–58. doi:10.1016/0167-2738(94)00184-T.
[27] P.C. McIntyre, Equilibrium Point Defect and Electronic Carrier Distributions near Interfaces in Acceptor-Doped Strontium Titanate, J. Am. Ceram. Soc. 83 (2000) 1129–1136. doi:10.1111/j.1151-2916.2000.tb01343.x.
[28] A. Tschöpe, S. Kilassonia, R. Birringer, The grain boundary effect in heavily doped cerium oxide, Solid State Ionics. 173 (2004) 57–61. doi:10.1016/j.ssi.2004.07.052.
[29] R.A. De Souza, The formation of equilibrium space-charge zones at grain boundaries in the perovskite oxide $SrTiO_3$, Phys. Chem. Chem. Phys. 11 (2009) 9939–9969. doi:10.1039/b905911n.
[30] A. Lindman, E.E. Helgee, G. Wahnström, Theoretical modeling of defect segregation and space-charge formation in the $BaZrO_3$ (210)[001] tilt grain boundary, Solid State Ionics. 252 (2013) 121–125. doi:10.1016/j.ssi.2013.04.008.
[31] E.E. Helgee, a. Lindman, G. Wahnström, Origin of Space Charge in Grain Boundaries of Proton-Conducting $BaZrO_3$, Fuel Cells. 13 (2013) 19–28. doi:10.1002/fuce.201200071.
[32] J. Kim, J. Yang, B. Kim, Y. Kim, Study of - Σ3 $BaZrO_3$ (210)[001] tilt grain boundaries using density functional theory and a space charge layer model, J. Ceram. Soc. Japan. 123 (2015) 245–249.
[33] P. Babilo, T. Uda, S.M. Haile, Processing of yttrium-doped barium zirconate for high proton conductivity, J. Mater. Res. 22 (2007) 1322–1330. doi:10.1557/jmr.2007.0163.
[34] S. Ricote, N. Bonanos, A. Manerbino, N.P. Sullivan, W.G. Coors, Effects of the fabrication process on the grain-boundary resistance in $BaZr_{0.9}Y_{0.1}O_{3-\delta}$, J. Mater. Chem. A. 2 (2014) 16107–16115. doi:10.1039/C4TA02848A.
[35] P.E. Blöchl, Projector augmented-wave method, Phys. Rev. B. 50 (1994) 17953–17979. doi:10.1103/PhysRevB.50.17953.
[36] G. Kresse, D. Joubert, From ultrasoft pseudopotentials to the projector augmented-wave method, Phys. Rev. B. 59 (1999) 1758–1775. doi:10.1103/PhysRevB.59.1758.
[37] J. Perdew, K. Burke, M. Ernzerhof, Generalized Gradient Approximation Made Simple., Phys. Rev. Lett. 77 (1996) 3865–3868. doi:10.1103/PhysRevLett.77.3865.
[38] H.J. Monkhorst, J.D. Pack, Special points for Brillouin-zone integrations, Phys. Rev. B. 13 (1976) 5188–5192. doi:10.1103/PhysRevB.13.5188.

[39] J.M. Polfus, T. Norby, R. Bredesen, Protons in Oxysulfides, Oxysulfates, and Sulfides: A First-Principles Study of La_2O_2S, $La_2O_2SO_4$, $SrZrS_3$, and $BaZrS_3$, J. Phys. Chem. C. 119 (2015) 23875–23882. doi:10.1021/acs.jpcc.5b08278.

[40] J.M. Polfus, M.-L. Fontaine, A. Thøgersen, M. Riktor, T. Norby, R. Bredesen, Solubility of transition metal interstitials in proton conducting $BaZrO_3$ and similar perovskite oxides, J. Mater. Chem. A. 4 (2016) 8105–8112. doi:10.1039/C6TA02377K.

[41] R.S. Alvim, I. Borges, D.G. Costa, A.A. Leit, Density-Functional Theory Simulation of the Dissociative Chemisorption of Water Molecules on the MgO (001) Surface, J. Phys. Chem. C. 116 (2012) 738–744. doi:10.1021/jp208007q.

[42] F. Iguchi, N. Sata, H. Yugami, Proton transport properties at the grain boundary of barium zirconate based proton conductors for intermediate temperature operating SOFC, J. Mater. Chem. 20 (2010) 6265. doi:10.1039/c0jm00443j.

[43] M. Shirpour, B. Rahmati, W. Sigle, P.A. Van Aken, R. Merkle, J. Maier, Dopant segregation and space charge effects in proton-conducting $BaZrO_3$ perovskites, J. Phys. Chem. C. 116 (2012) 2453–2461. doi:10.1021/jp208213x.

[44] M. Shirpour, G. Gregori, L. Houben, R. Merkle, J. Maier, High spatially resolved cation concentration profile at the grain boundaries of Sc-doped $BaZrO_3$, Solid State Ionics. 262 (2013) 860–864. doi:10.1016/j.ssi.2013.11.032.